

Speckle Control with a remapped-pupil PIAA-coronagraph

Frantz Martinache, Olivier Guyon, Christophe Clergeon & Celia Blain

National Astronomical Observatory of Japan, Subaru Telescope, Hilo, HI 96720, USA

frantz@naoj.org

ABSTRACT

The PIAA is a now well demonstrated high contrast technique that uses an intermediate remapping of the pupil for high contrast coronagraphy (apodization), before restoring it to recover classical imaging capabilities. This paper presents the first demonstration of complete speckle control loop with one such PIAA coronagraph. We show the presence of a complete set of remapping optics (the so-called PIAA and matching inverse PIAA) is transparent to the wavefront control algorithm. Simple focal plane based wavefront control algorithms can thus be employed, without the need to model remapping effects. Using the Subaru Coronagraphic Extreme AO (SCEXAO) instrument built for the Subaru Telescope, we show that a complete PIAA-coronagraph is compatible with a simple implementation of a speckle nulling technique, and demonstrate the benefit of the PIAA for high contrast imaging at small angular separation.

Subject headings: Astronomical Instrumentation — Extrasolar planets

1. Introduction

Contrast limits for the direct imaging of extrasolar planets from ground based adaptive optics (AO) observations are currently set by the presence of static and slow-varying aberrations in the optical path that leads to the science instrument (Marois et al. 2003). These aberrations, due to the non-common path error between the wavefront sensor and the science camera are responsible for the presence of long lasting speckles in the image. Because extrasolar planets are unresolved sources, it is difficult to discriminate them among these speckles. One family of techniques, called differential imaging, is aimed at calibrating out some of these static aberrations, by using either sky rotation (Angular Differential Imaging, or ADI), polarization (PDI), or wavelength dependence of the speckles (Spectral Differential Imaging or SDI). Of these, ADI (Marois et al. 2006) seems very well adapted to the problem of the detection of extrasolar planets, and has been successful, most notably producing the image of the planetary system around HR 8799 (Marois et al. 2008). ADI uses the rotation of the sky that naturally happens while tracking with an alt-azimuthal telescope around transit. The position of static and slowly varying speckles, tied to the diffraction by the pupil, remains stable over long timescales, while the image of planetary companions rotates around the one of the host star.

The rotation of the field only leads to sufficient linear displacement for angular separations of the order of one arcsecond. And in practice, below 0.5 arcsecond, the performance of ADI quickly degrades below the threshold where planets can be detected.

One way to complement ADI toward small angular separation, is to use a deformable mirror (DM) to modulate speckles and introduce the diversity that will distinguish them from genuine structures like planets and lumps in disks. This type of technique is regularly used for high contrast experiments (Guyon et al. 2010b), and appears as the technique of choice for a space borne mission dedicated to the direct imaging of high contrast planets. This is also the approach we propose to use for the detection of extrasolar planets at small angular separation during ground-based adaptive optics (AO) observations. In that scope we are integrating and testing the Subaru Coronagraphic Extreme AO (SCEExAO) project, whose optics have been described by Lozi et al. (2009) and Martinache et al. (2011).

In comparison with other extreme-AO projects (Macintosh et al. 2008; Beuzit et al. 2010), SCEExAO implements an aggressive PIAA-coronagraph using a remapping of the pupil (Guyon et al. 2005; Martinache et al. 2006) optimized for high-contrast detection at small angular separations (down to $1 \lambda/D$).

Laboratory high-contrast experiments relying on PIAA have demonstrated high contrast imaging capability in the 2-4 λ/D angular separation range, and achieved raw contrast of $\sim 10^{-7}$ and beyond (Guyon et al. 2010b; Kern et al. 2011; Belikov et al. 2011), that are several orders of magnitude beyond what a ground based instrument is expected to produce (Guyon 2005). From a reasonably good starting point, these experiments can produce high contrast images in a fairly small number of iterations, using electric field conjugation (EFC) framework that relies on an acute knowledge of the system’s complex amplitude response matrix (Give’On 2006; Bordé & Traub 2006). Ultimately, these techniques seem implementable at the telescope once an extreme AO system produces a continuous stream of stable high-Strehl images. They remain for now limited to the pampered environment of the laboratory. At this stage of its development (what is referred to as SCEExAO Phase 1), SCEExAO does not include a fully functioning high order wavefront sensor. The 32x32 DM it implements can be nevertheless used to actively generate speckle diversity and supplement ADI at small angular separations. SCEExAO phase 1 relies on iterative speckle nulling, to produce a dark hole (Malbet et al. 1995) in the field.

2. Speckle control within a PIAA-coronagraph

The Phase Induced Amplitude Apodization (PIAA) coronagraph (Guyon 2003) is a high-contrast imaging device that enables the detection of faint sources down to angular separation $\sim 1 \lambda/D$. A PIAA is made of a set of aspheric optics designed to apodize the pupil by geometrically redistributing the light while preserving the overall collimation of the beam for an on-axis source. Because it alters the pupil, the point spread function (PSF) of one such system is however no longer

translation invariant. On SCEExAO, the impact of the PIAA on the pupil is quite dramatic as it goes as far as filling the void left by the 30 % central obscuration of the Subaru Telescope pupil, to produce a apodized pupil better suited for high contrast imaging. The impact for off-axis sources is therefore also quite spectacular as it produces strongly elongated pineapple-shaped PSFs beyond a few λ/D (Lozi et al. 2009).

While successful wavefront control experiments using PIAA have already been reported (Guyon et al. 2010b; Kern et al. 2011; Belikov et al. 2011), these experiments have all been using a DM located downstream of the PIAA. The outer working angle (OWA) of this type of control is imposed by the total number of available actuators across one pupil diameter. By placing the DM downstream of the remapping optics, the OWA is reduced by a factor ~ 3 , due to the plate scale change induced by the remapping (Guyon et al. 2010b). The resulting $\sim 5\lambda/D$ OWA (since there are 32 actuators across the pupil) would be a very serious limitation for any direct imaging instrument. Instead, the SCEExAO project implements a complete PIAA-coronagraph, with a DM located before any of the remapping optics (cf. Fig. 1). After the focal plane mask, a copy of the PIAA optics plugged backwards (referred to as the inverse PIAA) is introduced to undo the remapping of the pupil after the focal plane mask. This setup allows to recover the wide field of view imaging capability of the instrument (Guyon & Roddier 2002; Guyon 2003).

The SCEExAO instrument is a flexible platform, installed after Subaru Telescope’s facility AO system, and designed to be used with the coronagraphic imager HiCIAO (Hodapp et al. 2008), and increase the size of the parameter space currently explored by the SEEDS survey (Tamura 2009; Tamura & SEEDS Team 2010), toward small angular separations. The infrared arm of SCEExAO alone (Martinache et al. 2011) supports multiple optical configurations (cf. Fig. 1), from straight-forward imager (with or without a focal plane mask), to a complete PIAA-coronagraph.

Lozi et al. (2009) have already demonstrated that the inverse PIAA once aligned and conjugated to the PIAA, indeed restores wide field of view imaging capability of the system, at least up to $20 \lambda/D$, which is beyond the outer working angle defined by the number of DM actuators across the instrument pupil. With this in mind, it seems reasonable to assume that the remapping optics should therefore be completely transparent for the wavefront control. The results presented in this paper demonstrate that indeed, with a complete PIAA-coronagraph (including the inverse PIAA), a simple wavefront control loop (speckle nulling) converges while being oblivious to the two remappings of the pupil.

2.1. Optical configurations of SCEExAO

To illustrate the impact of the remapping optics on the wavefront control, we use three distinct optical configurations of the SCEExAO infrared arm, shown in Fig. 1. The reader will observe that in its current implementation, the 32x32 MEMS DM of SCEExAO is not located in a pupil plane. This design was chosen for the simplicity of the optical layout, as well as to minimize the total

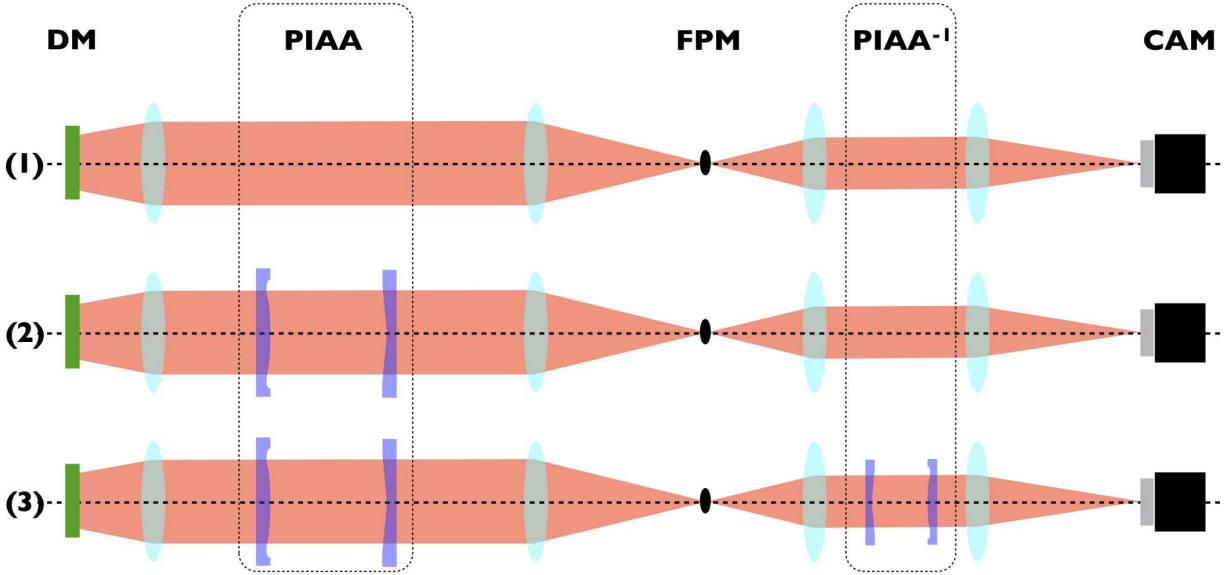


Fig. 1.— Schematic representation three of the possible optical configurations of the SCExAO bench used for the results presented in this paper. From left to right, the main components are highlighted as follows: the deformable mirror (labeled DM) located at an intermediate plane between pupil and image, the PIAA located in a collimated beam, the focal plane mask (labeled FPM) occulting the bright source observed with the system, the inverse PIAA (labeled PIAA^{-1}), also located in a collimated beam, in a plane conjugated with the PIAA so as to remap the pupil back to what it is when it enters the system, and finally, the detector (labeled CAM). From top to bottom, the three configurations are: (1) no remapping optics, equivalent to a Lyot coronagraph without a Lyot stop, (2) with PIAA only, and (3) with PIAA and inverse PIAA (the full coronagraph).

number of reflections in the system. The design however also has some drawbacks. First, it requires to be somewhat conservative with the beam size projected on the DM, to account for beam walk effects that would otherwise significantly vignette the field. The DM also needs to be horizontally tilted ($\sim 24^\circ$), so the density of actuators is not the same in horizontal and vertical directions. In practice, instead of illuminating all 32 available actuators across one pupil diameter, the beam spreads over a 27.2×24.8 actuator ellipse. SCEXAO can afford to have its DM away from the pupil since it is used downstream from an AO system that not only stabilizes the pupil, but also considerably reduces the total amount of aberrations the system needs to correct for.

While the DM is always part of the optical train, both the PIAA and the inverse PIAA are mounted on motorized stages that can swing in and out of the beam with excellent repeatability, thus allowing for quick alternance between three configurations: no remapping, PIAA only and PIAA + inverse PIAA (cf. Fig. 1). In a speckle control loop, the DM is used to introduce spatial frequencies that destructively interfere with speckles induced by wavefront aberrations from the input beam. The DM can also be used to create speckles, and in turn, provide a very instructive demonstration of how (cf. Fig. 2) aberrations propagate through the SCEXAO coronagraph.

Panel (a) of Fig. 2 shows the 32×32 volt-map sent to the DM for this experiment. In addition to the volt-map that has been determined to produce the best output wavefront in the absence of input aberrations (what will now be referred to as the DM flat-map), two sine waves of amplitude 0.4 radians and maximal spatial frequency (in the Nyquist sense) are added, along the horizontal and vertical directions. These additional sine functions on the DM create four bright speckles, clearly visible in the focal plane visible on Panel (b) of Fig. 2, in the absence of remapping optics. The oversized focal plane mask effectively hides the brightest area, but in the absence of Lyot stop, the diffraction by the spider arms bearing the secondary mirror of the telescope are left. Because the speckles result from the highest spatial frequency that can be introduced by the DM, their locations in the image also mark the edges of the region that can be controlled by the DM. In the absence of amplitude defects, appropriate actuation of the DM could clear the speckles over the entire $27.2 \times 24.8 \lambda/D$ box centered on the on-axis target. In practice, because the beam includes amplitude as well as phase defects, the DM can only operate over a half of this entire region. For the results reported in this work, we arbitrarily chose to work on the left-hand side of the field. Speckles located beyond $13.6 \lambda/D$ along the horizontal axis and $12.4 \lambda/D$ along the vertical axis simply will not be affected by the DM. Note that with a 0.04 arcsecond diffraction limit in the H-band, $12.4 \lambda/D$ on the Subaru Telescope closely matches the range of angular separation where ADI becomes usable ($12.4 \times 0.04 \simeq 0.5$ arcsecond).

2.2. Impact of the remapping optics

The introduction of the PIAA dramatically impacts the structure of these image (cf. panel (c) of Fig. 2). While the diffraction spikes created by the spider remain, most of the diffraction rings due to the sharp edge of the telescope pupil disappear, and are more effectively hidden by

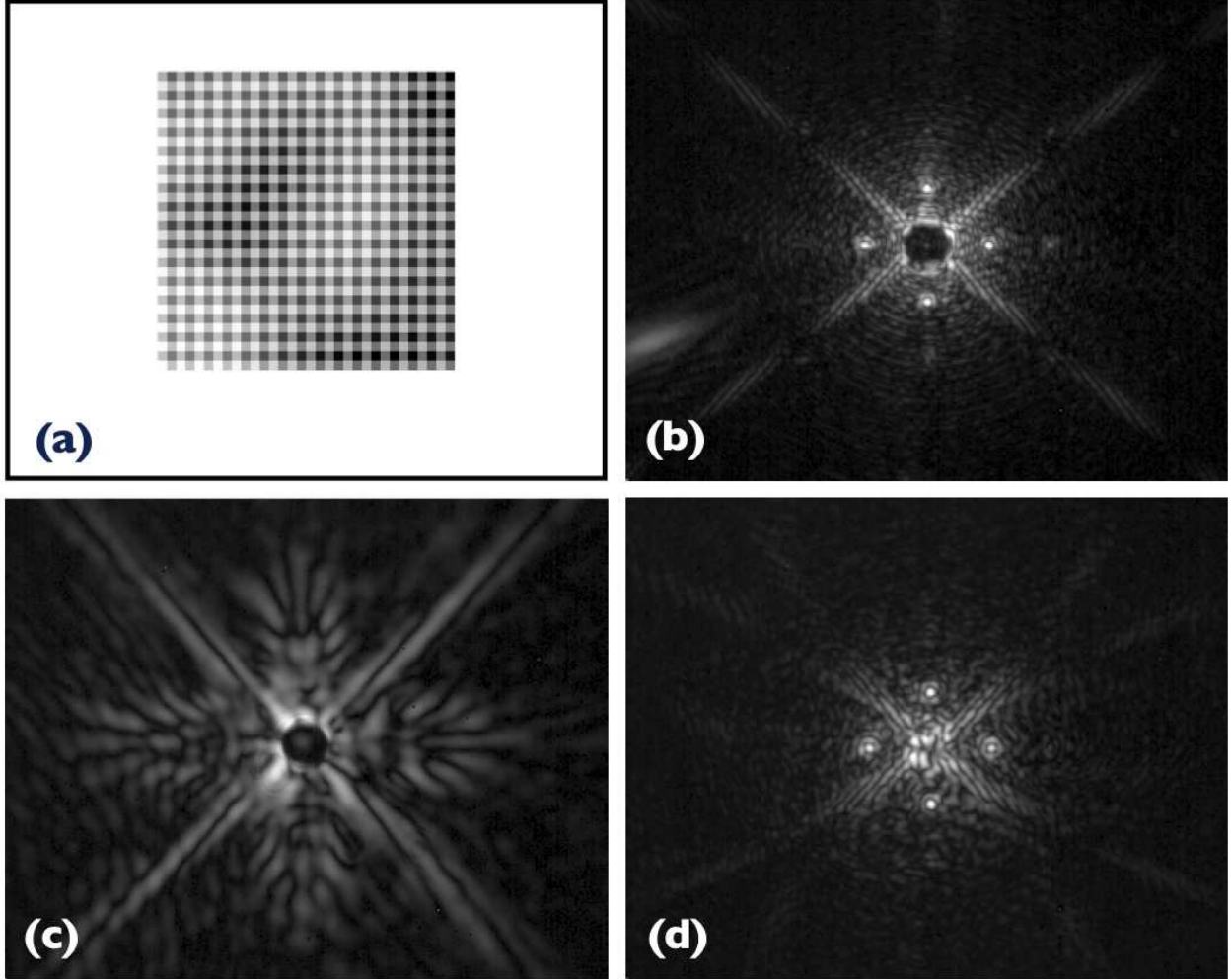


Fig. 2.— Demonstration of the effect of remapping optics on the image recorded by SCExAO’s science camera. Panel (a) shows the voltmap (ranging from 85 to 125 V) applied to the MEMS DM to produce the images that follow. Panels (b), (c) and (d) use a non-linear (square root) intensity scaling to highlight the faint diffraction structures surrounding the bright central area. Panel (b) shows the science camera image when the system is in configuration (1) (cf. Fig. 1). Panel (c) shows the dramatic effect of the PIAA on the focal plane image. Panel (d) shows the image obtained with the full coronagraph. Because the PIAA + inverse PIAA successfully restores the image of the off-axis speckles, it is expected that any type of focal-plane based wavefront control can ignore the presence of these remapping optics.

the focal plane mask whose size now better matches the on-axis PSF. Off-axis, however, the bright diffraction-limited images of introduced speckles are turned into complex pineapple-shaped aberrated structures. The benefit of the PIAA remapping will be better demonstrated when comparing the performance of the speckle nulling loop with and without using the remapping optics in Section 3.2.

The complete PIAA-coronagraph (configuration 3) includes after the focal plane mask, a copy of the PIAA optics mounted backwards to restore the geometry of the pupil back to what it was like before entering the coronagraph. From geometric optics principles only, one expects this restoration to be perfect, but diffraction and the presence of the occulting mask in the focal plane will impact the output wavefront. Panel (d) of Fig. 2 shows the resulting image: the bright off-axis speckles have been fully reconstructed by the inverse PIAA, and have recovered their airy-disk shape. The dark disk left by the focal plane mask that was visible in the other two images is no longer obvious, as the disk is remapped by the inverse PIAA.

The PIAA + inverse PIAA combination successfully restores the image of the off-axis speckles back into translation invariant copies of the central PSF. For speckles that would be sufficiently far from the edge of the focal plane mask, it is expected that any type of focal-plane based wavefront control can ignore the presence of these remapping optics. It is however not obvious for the speckles located nearby the original footprint of the focal plane mask that they should behave as simply. Section 3 will however show that speckle control can be achieved within the entire control region of the DM.

3. Speckle nulling results

3.1. The PIAA-coronagraph is transparent to the speckle control

To test the impact of the remapping (PIAA + inverse PIAA) optics for a focal plane based wavefront control loop, we use a simple iterative speckle nulling algorithm (Malbet et al. 1995), able to handle up to a dozen speckles simultaneously. This approach seems fairly inefficient in comparison with more sophisticated electric field conjugation (EFC) approaches that can achieve the same result in just a few iterations (Give’On 2006). Speckle nulling was nevertheless chosen because of its robustness and ease of implementation.

Indeed, complete EFC-based techniques rely on the knowledge of a response matrix that relates the complex amplitude of the on-axis source in the focal plane to the input wavefront. With an extreme AO loop effectively stabilizing the wavefront entering the coronagraph into something predictable, this matrix is likely to be quite stable, and therefore reliable. However in its first phase of deployment at the telescope, SCExAO does not include the fast wavefront sensor. The simple speckle nulling approach should, despite the presence of a dynamic atmospheric component, calibrate out the wavefront features responsible for the presence of static speckles in the images

(Guyon et al. 2010b).

Iterative speckle nulling works as follows: in a given image, up to n speckles are identified and their positions marked, relative to the central source. With a conventional imaging system, to each speckle position corresponds a two-component (x, y) spatial frequency on the DM, while its brightness indicates the amplitude a_0 of this spatial frequency. The only real unknown is the phase φ of each speckle, that can take any value between 0 and 2π . In the following four acquisitions, to each speckle is added a speckle probe of same amplitude a_0 , but each time with a different phase: 0, $\pi/2$, π and $3\pi/2$. The intensity of the four speckles resulting from the interference of the original speckle and the probes is used to determine its true phase φ_0 . For the next image, also used as the input for the next iteration, a spatial frequency of opposite phase $\varphi_0 + \pi$ and of amplitude $g \times a_0$, where g is the loop gain ($0.0 < g < 1.0$) is added so as to suppress the speckle.

The result of a series of 50 such speckle nulling iterations is presented in Fig. 3. The starting point, shown in the left panel, shows the structure of the speckles due to amplitude and phase defects that filtered through the coronagraph. One will observe that all ring like structures due to the sharp inner and outer edge of the pupil have been erased from the image, showing that the PIAA - focal plane mask - inverse PIAA combination achieves its purposes. Although faint (the average contrast over the entire control region is 2×10^{-3}), the most striking features can almost entirely be attributed to the spider arms bearing the secondary. After about 50 speckle nulling iterations (cf. right panel of Fig. 3), the average contrast inside the control region is brought down to 4×10^{-4} . The algorithm manages to suppress the diffraction features due to the spider arms, along which the gain in raw contrast is over 10^2 . Overall, the speckle nulling loop improves the contrast by a factor 10 over the entire control region.

3.2. The coronagraph relieves the wavefront control

Fig. 4 shows the DM voltmaps resulting from the speckle nulling algorithm for the Lyot-coronagraph (left panel) and the PIAA-coronagraph (right panel) configurations of SCExAO. Despite being ignorant of the pupil geometry, the speckle nulling produces a DM voltage induced phase pattern that resembles the original telescope simulator pupil.

In addition to the spider vanes, in the Lyot configuration, the algorithm attempts to cancel the diffraction rings induced by the sharp inner and outer edge of the pupil. The corresponding voltmap exhibits some sharp voltage changes from one actuator to its direct neighbor near the projection of these edges on the DM. Despite these sharp changes, this configuration fails to seriously cancel the innermost rings that would require more range than the DM can actually provide. The PIAA-coronagraph voltmap on the other hand, exhibits smoother features near the edge of the pupil, and only the effort to interfere with the speckle due to the spider vanes are really obvious. The coronagraph succeeds in relieving the wavefront control device by effectively suppressing a major fraction of the diffraction in the focal plane.

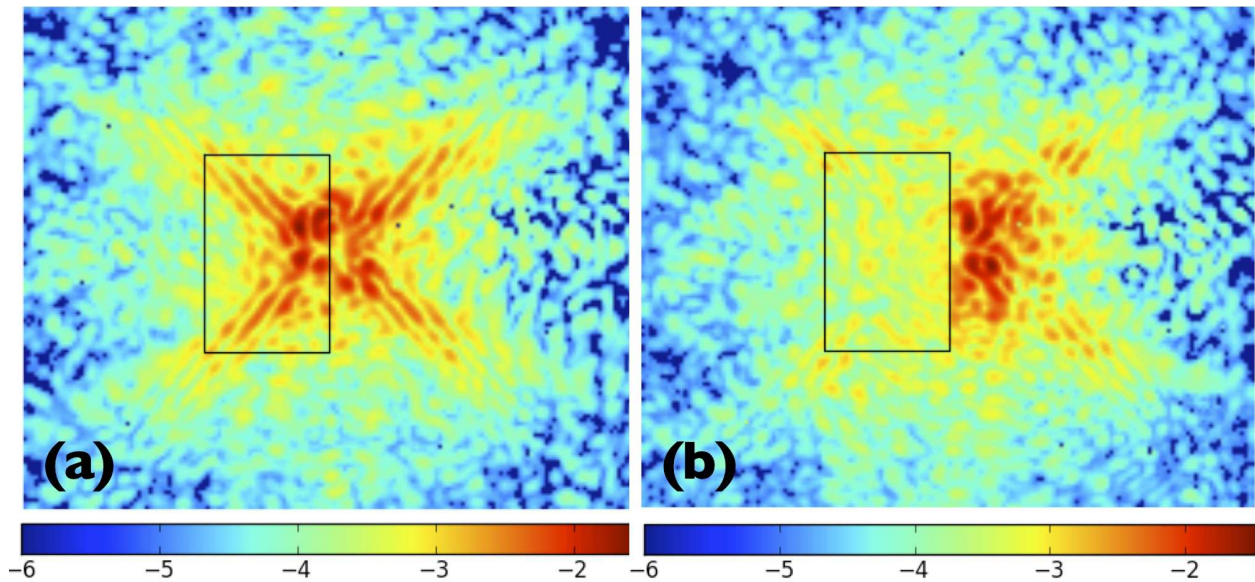


Fig. 3.— Example of high contrast result achievable with the SCEXAO coronagraph using a simple speckle nulling control loop. Panel (a) shows the starting point of the loop, with the deformable mirror in its nominal flat-map configuration. Note that in addition to some low-spatial frequency aberrations (created by a static turbulence plate), most of the speckles present at the starting point are located along the diffraction spikes created by the spider arms of the telescope pupil. Panel (b) shows the result of about 50 speckle nulling iterations, working on up to 10 speckles at a time, effectively clearing a box-shaped region of speckles, from 0 to $14 \lambda/D$ in the horizontal direction and within $\pm 14 \lambda/D$ in the vertical direction.

Note that the regions of the DM that obviously fall outside of the pupil do not need to be actuated at all. A more sophisticated DM control software should regularize the DM shape so as to preserve stroke on the DM.

3.3. Inner working angle

To further characterize the performance of the SCExAO coronagraph, and estimate its inner working angle, we look at the evolution of the throughput as a function of the position of the source relative to the focal plane across the field. While applying the DM voltage map resulting from a sequence of speckle nulling iterations, the source is translated along the horizontal axis. Fig. 5 shows six snapshots of the PSF as it moves across the "dark hole" created by the speckle nulling loop for the first $5 \lambda/D$ away from on-axis. Within $1 \lambda/D$ and a little beyond, ring-like structures remain erased by the coronagraph. At $2 \lambda/D$, the core of the PSF clears the coronagraph and diffraction rings re-appear in the image. Beyond $2 \lambda/D$, the structure of the PSF is essentially translation invariant, and only the shadow of the focal plane mask betrays the presence of the coronagraph.

To complete this qualitative analysis of post coronagraph images, Fig. 6 shows a curve of the system throughput, integrated over the left hand side of the field, as the sources is moved across the entire $14 \lambda/D$ control region, and slightly beyond. The 100 % throughput reference is determined on-axis by removing the focal plane mask. Matching our qualitative description of snapshots in Fig. 5, we confirm that within $1 \lambda/D$, the throughput only varies at the percent level. The most rapid variation of throughput happens around $2 \lambda/D$, where the PSF core clears the focal plane mask as shown in Fig. 5: the throughput quickly rises from a few percent to 60 %.

One convenient definition of the inner working angle (IWA) of a coronagraph is the angular separation at which its transmission reaches 50 % (Guyon et al. 2006). According to the measurements summarized in Fig. 6, SCExAO's current IWA is $2.2 \lambda/D$. The focal plane mask currently used is 40 % oversized, compared to the $1.6 \lambda/D$ IWA the PIAA optics have been manufactured for. It will therefore be replaced before SCExAO's next observing run.

4. Conclusion

We have, for the first time, demonstrated focal plane wavefront control capability in a complete PIAA - focal plane mask - inverse PIAA system. Using a simple iterative speckle nulling algorithm, we successfully produced a high contrast region in the field (the so-called dark hole), and therefore confirmed that the complete set of remapping optics (PIAA and inverse PIAA) are transparent to the focal plane based wavefront control. We have also confirmed that the outer working angle allowable by the number of actuators of the deformable mirror is preserved during the double remapping. This implies that PIAA-type coronagraphs can be very well be used on ground and

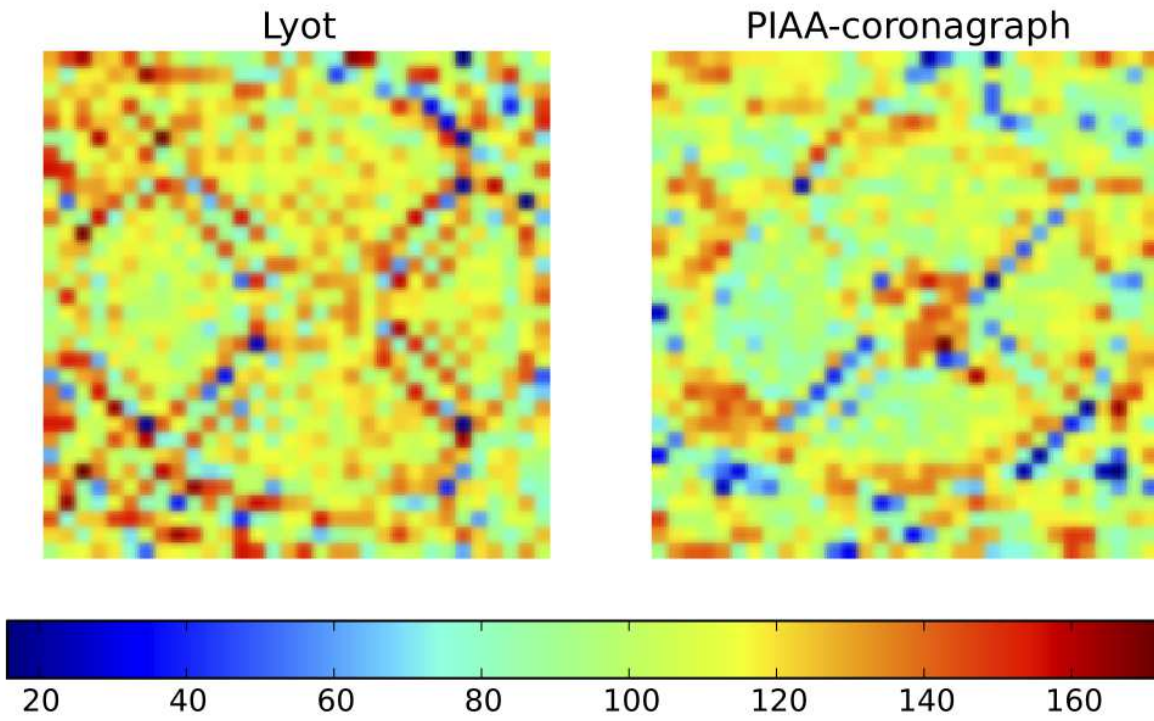


Fig. 4.— Speckle nulling voltmaps for configurations (1) Lyot-coronagraph and (3) PIAA-coronagraph of SCEXAO (cf. Fig. 1).

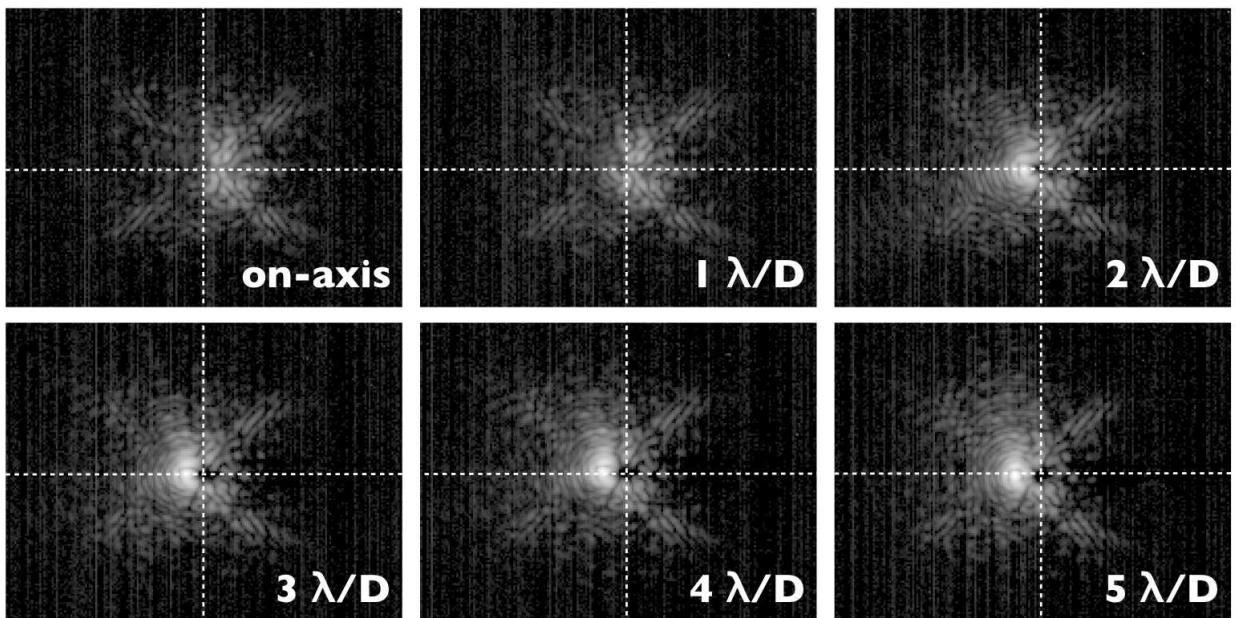


Fig. 5.— Evolution of the PSF as a function of off-axis position near the focal plane mask from on-axis to $5 \lambda/D$ off-axis. At $2 \lambda/D$, the core of the PSF has almost entirely cleared the focal plane mask, and the diffraction rings associated with it become visible again. Beyond $3 \lambda/D$, the PSF morphology is essentially translation invariant. Images use a common logarithmic intensity scale to reveal both bright and faint features of the PSFs.

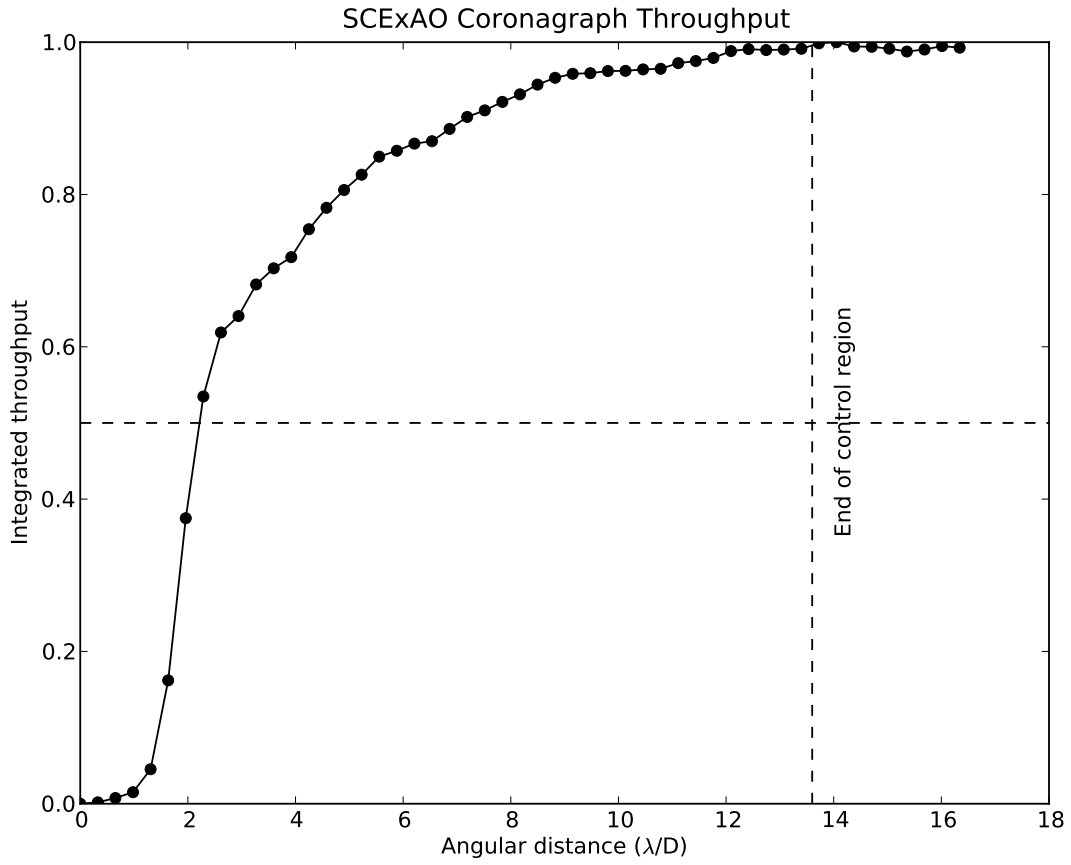


Fig. 6.— Throughput of the SCEExAO coronagraph as a function of angular separation. Using an iterative speckle nulling algorithm, the voltage map that cancels speckles within the control region of the DM has been identified. This curve shows how the throughput of the coronagraph evolves as the source is progressively translated off-axis, across the entire $14 \lambda/D$ wide control region.

space-based telescopes with no loss of outer working angle and do not require complex wavefront control algorithms. High performance high efficiency coronagraphy therefore does not translate into increased system complexity.

Note that while we tested PIAA with a large mask imposing a $2.2 \lambda/D$ inner working angle), the conclusions of this paper will hold for more IWA-optimized PIAA coronagraphs, including the PIAACMC (Guyon et al. 2010a) that exhibit $IWA < 1\lambda/D$. Combined with focal plane based wavefront control to what this paper demonstrates, such aggressive designs make coronagraphy onboard small telescopes (~ 2 meters) in space a relevant option for the direct detection of extrasolar planets. They also offer the potential for imaging reflected light planets at very small separation with the forthcoming generation of extremely large telescopes.

One should also note that the moderate contrast level results presented here were achieved in monochromatic light. Yet at the 10^{-4} to 10^{-6} raw contrast level ground-based extreme AO systems will give access to, speckle nulling remains a valid option in polychromatic light. The coronagraph currently in place in SCExAO does not take into account the spider vanes in the pupil, while these are responsible for most of the light observed in the final focal plane of the instrument. Consequently, the wavefront control algorithm must use pupil phase introduced by the deformable mirror to remove, over half of the focal plane, light diffracted by the spider vanes, as shown in figure 4. This approach is simply not suitable in a broad spectral band, and the SCExAO coronagraph will be updated to a PIAACMC type coronagraph to solve this issue.

Finally, while the results presented in this paper demonstrate the raw contrast required for ground-based system, it is unclear to which extent the approach adopted in this work is suitable for the $\sim 10^{-9}$ contrast level that future space-based missions hope to reach in order to image and study Earth-like planets. While remapping propagation effects specific to the PIAA coronagraph can be included in the wavefront control algorithm (Krist et al. 2011), it is unknown to which extent such effects need to be accounted for. The approach presented in this paper should be tested, both in simulations and in laboratory experiments, at higher contrast than required for a ground-based system. This work will be conducted over the next two years on existing PIAA coronagraph testbeds.

REFERENCES

- Belikov, R., Pluzhnik, E., Witteborn, F. C., et al. 2011, in Society of Photo-Optical Instrumentation Engineers (SPIE) Conference Series, Vol. 8151, Society of Photo-Optical Instrumentation Engineers (SPIE) Conference Series
- Beuzit, J.-L., Feldt, M., Mouillet, D., et al. 2010, in In the Spirit of Lyot 2010
- Bordé, P. J. & Traub, W. A. 2006, ApJ, 638, 488
- Give'On, A. 2006, PhD thesis, Princeton University

- Guyon, O. 2003, *A&A*, 404, 379
- Guyon, O. 2005, *ApJ*, 629, 592
- Guyon, O., Martinache, F., Belikov, R., & Soummer, R. 2010a, *ApJS*, 190, 220
- Guyon, O., Pluzhnik, E., Martinache, F., et al. 2010b, *PASP*, 122, 71
- Guyon, O., Pluzhnik, E. A., Galicher, R., et al. 2005, *ApJ*, 622, 744
- Guyon, O., Pluzhnik, E. A., Kuchner, M. J., Collins, B., & Ridgway, S. T. 2006, *ApJS*, 167, 81
- Guyon, O. & Roddier, F. 2002, *A&A*, 391, 379
- Hodapp, K. W., Suzuki, R., Tamura, M., et al. 2008, in *Society of Photo-Optical Instrumentation Engineers (SPIE) Conference Series*, Vol. 7014, *Society of Photo-Optical Instrumentation Engineers (SPIE) Conference Series*
- Kern, B., Guyon, O., Give'On, A., Kuhnert, A., & Niessner, A. 2011, in *Society of Photo-Optical Instrumentation Engineers (SPIE) Conference Series*, Vol. 8151, *Society of Photo-Optical Instrumentation Engineers (SPIE) Conference Series*
- Krist, J. E., Belikov, R., Pueyo, L., et al. 2011, in *Techniques and Instrumentation for Detection of Exoplanets V*. Edited by Shaklan, Stuart. *Proceedings of the SPIE*, Volume 8151, pp. 81510E-81510E-16 (2011)., Vol. 8151
- Lozi, J., Martinache, F., & Guyon, O. 2009, *PASP*, 121, 1232
- Macintosh, B. A., Graham, J. R., Palmer, D. W., et al. 2008, in *Society of Photo-Optical Instrumentation Engineers (SPIE) Conference Series*, Vol. 7015, *Society of Photo-Optical Instrumentation Engineers (SPIE) Conference Series*
- Malbet, F., Yu, J. W., & Shao, M. 1995, *PASP*, 107, 386
- Marois, C., Doyon, R., Nadeau, D., Racine, R., & Walker, G. A. H. 2003, in *EAS Publications Series*, Vol. 8, *EAS Publications Series*, ed. C. Aime & R. Soummer, 233–243
- Marois, C., Lafrenière, D., Doyon, R., Macintosh, B., & Nadeau, D. 2006, *ApJ*, 641, 556
- Marois, C., Macintosh, B., Barman, T., et al. 2008, *Science*, 322, 1348
- Martinache, F., Guyon, O., Garrel, V., et al. 2011, in *Society of Photo-Optical Instrumentation Engineers (SPIE) Conference Series*, Vol. 8151, *Society of Photo-Optical Instrumentation Engineers (SPIE) Conference Series*
- Martinache, F., Guyon, O., Pluzhnik, E. A., Galicher, R., & Ridgway, S. T. 2006, *ApJ*, 639, 1129

Tamura, M. 2009, in American Institute of Physics Conference Series, Vol. 1158, American Institute of Physics Conference Series, ed. T. Usuda, M. Tamura, & M. Ishii, 11–16

Tamura, M. & SEEDS Team. 2010, in In the Spirit of Lyot 2010